A variational method for tomographic reconstruction with few views

Isabelle Abraham, Romain Abraham, Maïtine Bergounioux

Inverse Problems in Science and Engineering
Vol. 00, No. 00, July 2012, 1–25

RESEARCH ARTICLE

A variational method for tomographic reconstruction with few views

I. Abraham [a] R. Abraham[b] and M. Bergounioux[b]*

[a] *CEA Ile de France- BP 12, 91680 Bruyères le Châtel, France* ; [b] *Université d'Orléans, UFR Sciences, MAPMO, UMR 7349, Route de Chartres, BP 6759, 45067 Orléans cedex 2, France*

(*v1.2 released July 3, 2012*)

In this article, we focus on tomographic reconstruction. The problem is to determine the shape of the interior interface using a tomographic approach while very few X-ray radiographs are performed. We present a variational model and numerical analysis. We use a modified Nesterov algorithm to compute the solution. Numerical results are presented.

Keywords: Inverse problem, Tomography, Variational model

AMS Subject Classification: 49N45, 35A15,65J22,94A08

1. Introduction

In this article, we focus on a specific application of tomographic reconstruction for a physical experiment whose goal is to study the behavior of a material under a shock. The experiment consists in causing the implosion of the hull of some material (usually, a metal) using surrounding explosives. The problem is to determine the density and the interior interface at a specific moment of the implosion. For this purpose, very few X-ray radiographs are performed, and the density of the object must then be reconstructed using a tomographic approach (see Figure 1.1).

In [1] we mentioned that several techniques exist for tomographic reconstruction, providing an analytic formula for the solution (see for instance [15] or [13]) as soon as a large number of projections of the object, taken from different angles, are available. There is a huge literature about theoretical and practical aspects of the problem of reconstruction from projections, the applications of which concern medicine, optics, material science, astronomy, geophysics, and magnetic resonance imaging (see [7]). When only few projections are known, these methods cannot be used directly, and some alternative methods have been proposed to reconstruct the densities (see for instance [19]).

As in any tomographic reconstruction process, this problem leads to an ill-posed inverse problem. As X-rays must cross a very dense object and only a few number of them arrive at the detector, it is therefore necessary to add some amplification devices and very sensitive detectors, which cause a high noise level [25, 26] .

*Corresponding author. Email: maitine.bergounioux@univ-orleans.fr

ISSN: 1741-5977 print/ISSN 1741-5985 online

DOI: 10.1080/1741597YYxxxxxxxx
http://www.informaworld.com

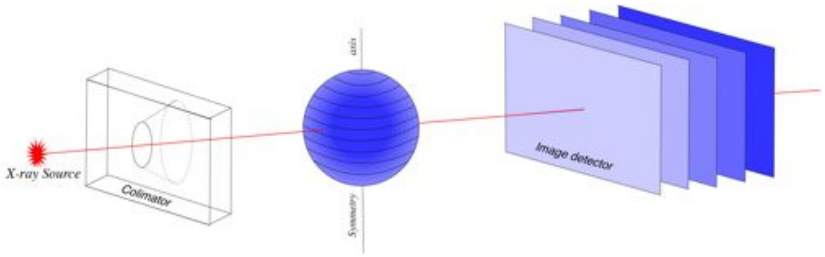

Figure 1.1. Tomography experiment

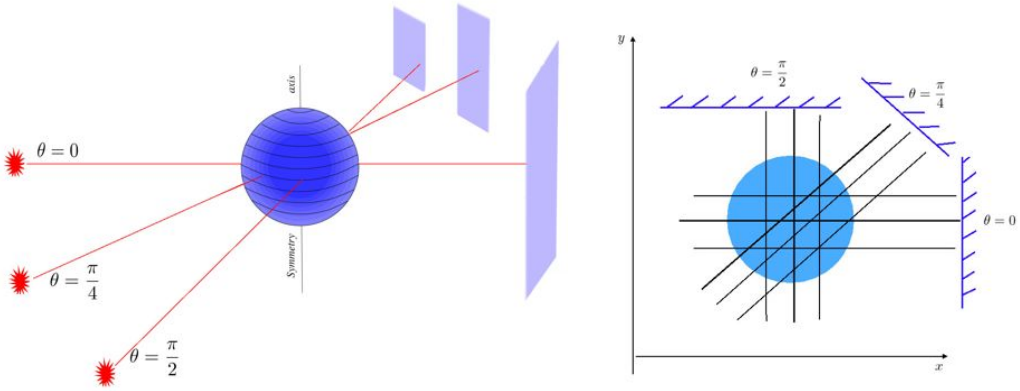

Figure 1.2. Different projections around the tomography axis

The tomographic reconstruction with few views problem has been widely studied. If a large number of radiographs is available, we can use several efficient methods that lead to exact formulas to compute the solution (see [22] or [15]).

Missing data problems can been studied with such methods as well ([22], chapter 6 or [27]). It is the case, for example, when the object is measured on a subset of its support (so-called inner problem, see for example [12]). These techniques, as, for instance, the back-filtered projection (in the full case) or the back-projection for the projection derivatives (in the missing data case [24]) require a fine sampling of measures (here radiographs) to be performing ([22], chapter 4). Therefore, they are not useful in the case where few projection data are available.

The number of available projections (views) is closely related to the ill-posedness of the reconstruction problem. Indeed, the smaller the number of data is, the larger is the kernel of the related operator. Roughly speaking, there are an infinity of solutions and this infinity is linked to the kernel dimension. Some methods have been proposed that allow a partial reconstruction of the object [19]. In the case where we deal with specific objects there exists methods selecting a solution with respect to some prior : in [18], [17] the authors use a bayesian model while an optimization approach is used in [6],[5] where the problem is modelled as a minimal cost flow problem.

In [1] we have assumed that the components of the initial physical setup (object, hull, explosives, etc) are axially symmetric and remain as such during the implosion process. High speed image capture provides a snapshot of the deformation of an object by X-ray radiography. Since this object is assumed to be axially symmetric, a single radiograph suffices in theory to reconstruct the 3D object. The inverse

problem remains ill-posed : existence and uniqueness of a solution are ensured but there is a lack of stability. However, interesting results have been obtained with a variational method ([1, 8]).

In the present paper, we do not assume that the object is axially symmetric any longer but we have more than one radiograph. However, due to the experimental setup, we only deal with very few radiographs, taken from three angles that we suppose to be $0, \frac{\pi}{4}$ and $\frac{\pi}{2}$ for sake of simplicity. So the prior to choose is not straightforward. The previously quoted methods are efficient as soon as we have much more data sets (projections) than we have. In this paper we propose to use a variational method involving priors that are not necessarily consistent with the physical point of view. Looking for more appropriate models will be done in forthcoming works.

The paper is organized as follows. We first present the direct and inverse problems with some classical methods that are not fruitful in this context. Next section is devoted to the study of a variational model both from the theoretical and numerical points of view. We present a generic algorithm. The last section is devoted to the numerical experiments: discretization process, algorithmic tricks and results.

2. Mathematical modelling of the direct problem

In what follows, we assume that the X-sources are far enough from the object so that we may assume that the X-rays are parallel. Therefore we can separate the horizontal planes and reconstruct them independently (see Figure 2.1).

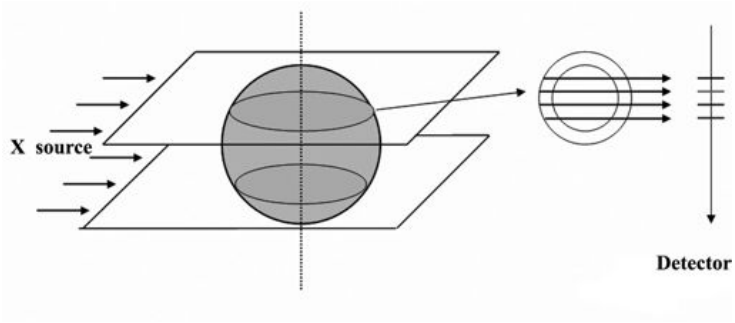

Figure 2.1. Parallel X-rays : the information along a detector segment depends on a planar slice of the object.

We recall [1] that radiography measures the attenuation of X-rays through the object. Let I_0 denote the intensity of the incident X-rays flux. Then, the measured flux I at a point M of the detector is given by

$$I = I_0 e^{-\int_\Delta \mu(\ell) d\ell},$$

where the integral operates along the ray Δ that reaches the point M of the detector, $d\ell$ is the infinitesimal element of length along the ray, and μ is the linear attenuation coefficient. Considering the Neperian logarithm of this attenuation permits to deal rather with linear operators, and the linear mapping

$$H : (\Delta, \mu) \longmapsto H(\Delta, \mu) := \int_\Delta \mu(\ell)\, d\ell$$

is called the *projection operator*. Let us fix the z -coordinate and set $\mu_z : (x, y) \mapsto$

$\mu(x,y,z)$. The operator H restricted to any horizontal plane (z constant) coincides with the bidimensional Radon transform of μ_z. Let us recall its definition [21] :

Definition 2.1: Assume $n \geq 2$ and define $\mathbf{S}^{n-1}$ as the unit sphere of $\mathbb{R}^n$. For any function $f \in \mathcal{S}(\mathbb{R}^n)$ the Radon transform R is defined as

$$\begin{aligned} Rf : \mathbf{S}^{n-1} \times \mathbb{R} &\to \mathbb{R} \\ (\zeta, s) &\mapsto \int_{x.\zeta=s} f(x)dx = \int_{\zeta^\perp} f(s\zeta + y)dy \ . \end{aligned}$$

where $x.\zeta$ stands for $\mathbb{R}^n$ usual inner product and $\zeta^\perp$ is the orthogonal subspace to $\mathbb{R}\zeta$.

Here $\mathcal{S}(\mathbb{R}^n)$ is the Schwartz space of $\mathcal{C}^\infty$, rapidly decreasing functions. For any $f \in \mathcal{S}(\mathbb{R}^n)$, Rf belongs to $\mathcal{S}(\mathbf{S}^{n-1} \times \mathbb{R})$. If $n = 2$, the Radon transform of a function $f \in \mathcal{S}(\mathbb{R}^2)$ reads

$$\forall \theta \in [0, \pi[, \ \forall s \in \mathbb{R} \qquad Hf(\theta, s) = \int_{-\infty}^{+\infty} f(t\sin(\theta) + s\cos(\theta), -t\cos(\theta) + s\sin(\theta))\, dt$$

and the relation between R and H is : $Hf(\theta, s) = Rf\,(\zeta, s)$, where $\zeta = (\cos\theta, \sin\theta)$. So, the reconstruction of the object requires the inversion of the Radon transform restricted to any horizontal slice. Therefore, we focus now on the inversion in the 2D framework. We assume that the object is completely represented by its attenuation coefficient μ proportional to its density $\rho : \mathbb{R}^2 \to \mathbb{R}$. We assume in addition that ρ vanishes outside an (2D) open disk $\Omega = B_{\|.\|_2}(0, a)$ of center 0 and radius a. Therefore, the support of ρ is included in Ω. Here $\|.\|_2$ denotes the euclidean norm. In what follows, we call $\mathcal{C}_c^0(\Omega)$, the space of continuous functions with compact support in Ω.

Remark 1: As $\rho = 0$ outside $\Omega \subset]-a, a[\times]-a, a[$, then

$$\int_\Omega \rho(x, y)\, dx\, dy = \int_{-a}^{a}\int_{-a}^{a} \rho(x, y)\, dx\, dy$$

as soon as the integrals are defined.
For any $\theta \in [0, \pi[$ the Radon transform of $\rho \in \mathcal{C}_c^0(\Omega)$, is defined as :

$$\begin{aligned} H\rho(\theta, s) &= \int_{-\infty}^{+\infty} \rho(t\sin(\theta) + s\cos(\theta), -t\cos(\theta) + s\sin(\theta))\, dt \\ &= \int_{-a}^{+a} \rho(t\sin(\theta) + s\cos(\theta), -t\cos(\theta) + s\sin(\theta))\, dt. \end{aligned}$$

It has a compact support included in $]-a, a[$. For every $\theta \in [0, \pi[$ let us note H_θ the operator defined as

$$\begin{aligned} H_\theta\rho : \mathbb{R} &\to \mathbb{R} \\ s &\mapsto H\rho(\theta, s) \ . \end{aligned}$$

Therefore

$$H_0\rho(s) = \int_{-\infty}^{+\infty} \rho(t, s)\, dt = \int_{-a}^{+a} \rho(t, s)\, dt \ . \tag{2.1}$$

Let Γ_θ be the rotation of center $(0,0)$ and angle θ:

$$\forall \rho \in \mathcal{C}_c^0(\Omega), \quad \Gamma_\theta \rho(x,y) = \rho(x\cos(\theta) + y\sin(\theta), -x\sin(\theta) + y\cos(\theta)),$$

so that the projection operator with angle $\theta \in [0,\pi]$ is

$$H_\theta = H_0 \circ \Gamma_\theta : \mathcal{C}_c^0(\Omega) \to \mathcal{C}_c^0(]-a,a[).$$

We may extend the operator H_0 to $L^2(\Omega)$ by density with next proposition. In what follows, for any subset E of $\mathbb{R}^s$, $(\cdot,\cdot)_{L^2(E)}$ denotes the $L^2(E)$ inner product and $\|\cdot\|_{L^2(E)}$ the $L^2(E)$ hilbertian norm. We note $(\cdot,\cdot)_2$ and $\|\cdot\|_2$ when there is no ambiguity.

Proposition 2.2: *The operator H_θ is a bounded linear operator from $\left(\mathcal{C}_c^0(\Omega), \|.\|_{L^2(\Omega)}\right)$ to $\left(\mathcal{C}_c^0(]-a,a[), \|.\|_{L^2(]-a,a[)}\right)$.*

Proof: Let be $\rho \in \mathcal{C}_c^0(\Omega)$. Then

$$\|H_0\rho\|_{L^2}^2 = \int_{-a}^{a} \left| \int_{-a}^{a} \rho(x,y)dx \right|^2 dy = \int_{-a}^{a} \left(\rho(.,y)\ , 1_{]-a,a[}\right)_{L^2(]-a,a[)}^2 dy \leq 2a\|\rho\|_{L^2}^2$$

by Cauchy-Schwarz inequality. As Γ_θ is an isometry we have the same result for H_θ. □

We extend H_θ on $L^2(\Omega)$ by density arguments and we denote similarly the extended operator. We can define the adjoint operator of H_0: $H_0^* : L^2(]-a,a[) \longrightarrow L^2(\Omega)$ such that

$$\forall (v,\rho) \in L^2(]-a,a[) \times L^2(\Omega) \quad (v\ , H_0\rho)_{L^2(]-a,a[)} = (H_0^* v\ , \rho)_{L^2(\Omega)}\,.$$

Proposition 2.3: *The adjoint operator of H_0 is given by*

$$\begin{aligned} H_0^* : L^2(]-a,a[) &\longrightarrow L^2(\Omega) \\ H_0^* v(x,y) &:= 1_\Omega(x,y)v(y), \text{ for a.e. } y \end{aligned}$$

where 1_Ω is the indicator function of Ω : $1_\Omega(x,y) = \begin{cases} 1 \text{ if } (x,y) \in \Omega \\ 0 \text{ else} \end{cases}$

Proof: Let $v \in L^2(]-a,a[)$, $\rho \in L^2(\Omega)$ and (ρ_n) be a sequence of $\mathcal{C}_c^0(\Omega)$ functions that converges to ρ in $L^2(\Omega)$. We get for every $n > 0$

$$(H_0^* v\ , \rho_n)_{L^2(\Omega)} = (v\ , H_0\rho_n)_{L^2(]-a,a[)} = \int_{-a}^{a} v(y) H_0\rho_n(y)\, dy = \int_\Omega v(y)\rho_n(x,y)\, dx\, dy\,.$$

Passing to the limit as $n \to +\infty$ gives the result. □

We deduce H_θ^* easily : $H_\theta^* = (H_0 \circ \Gamma_\theta)^* = \Gamma_\theta^* \circ H_0^* = \Gamma_{-\theta} \circ H_0^*$.

3. A variational model

In what follows, $\{\theta_0, \theta_1, \ldots, \theta_{p-1}\}$ denotes the p acquisition angles (in $[0,\pi[$). The measured data are $\pi_i (:= H_i\rho) \in L^2(]-a,a[)$ where $H_i := H_{\theta_i}$, $i = 0, \cdots, p-1$. It is easy to see that, if a solution exists, it is not necessarily unique.

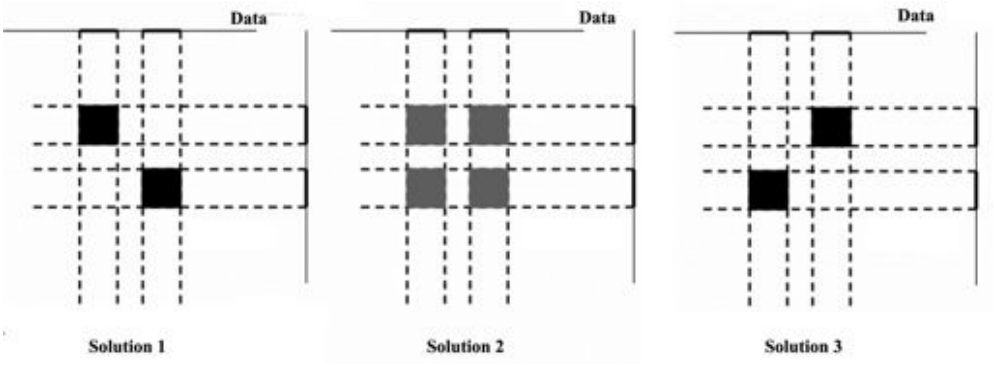

Figure 3.1. Example of three different solutions for the same 2-views data set .

As already mentioned, it is hopeless to get exact inversion formulas to solve

$$H_i\rho = \pi_i,\ i = 0, \cdots, p-1.$$

So we rather use a least square approach to minimize $\sum_{i=0}^{p-1} \|H_i\rho - \pi_i\|^2_{L^2(]-a,a[)}$. As the kernel of H_i may be quite large , the space $\mathcal{N} = \bigcap_{i=0}^{p-1} \ker H_i$ may be not reduced to $\{0\}$ and the functional is not coercive, not strictly convex. More precisely, if any minimizing sequence lies in $\mathcal{N}$ it is not possible to prove its convergence. Moreover, even if we get a solution, we dot not have uniqueness. Therefore, we have to add some prior information on ρ . It is classical to consider the total variation of functions, which is an efficient tool to reduce noise, as a penalization term.

3.1. *Functional framework*

In what follows, E is an open bounded subset of $\mathbb{R}^n$. We recall here the definition of the the space of bounded variation functions (see [3]):

$$BV(E) = \{u \in L^1(E) \mid \Phi(u) < +\infty\},$$

where

$$\Phi(u) = \sup\left\{\int_E u(x)\,\mathrm{div}\ \xi(x)\,dx \mid \xi \in \mathcal{C}^1_c(E),\ \|\xi\|_\infty \leq 1\right\}. \tag{3.2}$$

The application Φ is a semi-norm and the space $BV(E)$, endowed with the norm $\|u\|_{BV} = \|u\|_{L^1} + \Phi(u)$, is a Banach space. The derivative in the sense of the distributions of every $u \in BV(E)$ is a bounded Radon measure, denoted Du, and $\Phi(u) = \int_E |Du|$ is the total variation of Du. We next recall standard properties of bounded variation functions (see [2, 3]).

Proposition 3.1: *Let E be an open subset of $\mathbb{R}^n$ with Lipschitz compact boundary.*

(1) For every $u \in BV(E)$, the Radon measure Du can be decomposed into $Du = Du\,dx + D^s u$, where $Du\,dx$ is the absolutely continuous part of Du with respect of the Lebesgue measure and $D^s u$ is the singular part.

(2) The mapping $u \mapsto \Phi(u)$ is lower semi-continuous (denoted in short lsc) from $BV(E)$ to $\mathbb{R}^+$ for the $L^1(E)$ topology.

(3) $BV(E) \subset L^{1^*}(E)$ with continuous embedding, where $1^* := \dfrac{n}{n-1}$

(4) $BV(E) \subset L^p(E)$ with compact embedding, for every $p \in [1, 1^*)$.

Remark 1 : As the set Ω satisfies the assumptions of Proposition 3.1 with $n = 2$, we may study the Radon operator restricted to $BV(\Omega) \subset L^2(\Omega)$.
Moreover we may extend the total variation operator to $L^2(\Omega)$ as follows:

$$\begin{aligned} \tilde{\Phi} : L^2(\Omega) &\longrightarrow [0, +\infty] \\ u &\mapsto \begin{cases} \Phi(u) \text{ if } u \in BV(\Omega) \\ +\infty \text{ else.} \end{cases} \end{aligned}$$

In the sequel we denote similarly $\tilde{\Phi}$ and Φ.

3.2. *A variational model*

We now consider the following minimization problem:

$$(\mathcal{P}) \ : \min_{\rho \in BV(\Omega)} J_\varepsilon(\rho)$$

where $\|\cdot\|_2$ stands for the $L^2(\Omega)$ or $L^2(]-a, a[)$ norm and

$$J_\varepsilon(\rho) := \frac{1}{2} \sum_{k=0}^{p-1} \|H_k \rho - \pi_k\|_2^2 + \tau \Phi(\rho) + \frac{\varepsilon}{2} \|L\rho\|_2^2 \ , \tag{3.3}$$

with $\tau > 0$ and $\varepsilon > 0$. Let us comment the different terms:

- The first one : $\displaystyle\sum_{k=0}^{p-1} \|H_k \rho - \pi_k\|_2^2$ is the fitting data term.
- The term $\tau\, \Phi(\rho)$ is a total variation penalization term: it allows to reduce the noise. The parameter τ can be tuned with respect to the noise level.
- The last one $\dfrac{\varepsilon}{2}\|L\rho\|_2^2$ is a mathematical tool that forces the strict convexity and coercivity of the cost functional and gives existence and uniqueness of a solution. The parameter ε should be chosen as small as possible. L is a linear continuous bijective operator from $L^2(\Omega)$ to $L^2(\Omega)$. We may choose for example $L = Id_{L^2(\Omega)}$ the identity operator (what we have done for the numerical tests of last section). However, this choice makes poor physical meaning. We may rather think of convolution operator (high-pass or low-pass filter for example). As L is a $L^2(\Omega)$-isomorphism we get the existence of $\kappa > 0$ such that

  $$\|Lu\|_2^2 \geq \kappa \|u\|_2^2 \ ,$$

  as well. Note that if $L = Id_{L^2(\Omega)}$ then $\kappa = 1$.

With Remark **1**, problem $(\mathcal{P})$ writes

$$(\mathcal{P}) \ : \inf_{\rho \in L^2(\Omega)} J_\varepsilon(\rho) := F_\varepsilon(\rho) + \tau \Phi(\rho)$$

where F_ε is defined on $L^2(\Omega)$ by :

$$F_\varepsilon(\rho) := \frac{1}{2}\sum_{k=0}^{p-1}\|H_k\rho - \pi_k\|_2^2 + \frac{\varepsilon}{2}\|L\rho\|_2^2. \tag{3.4}$$

Remark 2 : It is known [20] that any solution to problem $\min\limits_{\rho\in BV(\Omega)} F_\varepsilon(\rho)$ is a solution to $\min\{\|L\rho\|_2 \mid \rho\in BV(\Omega)\ , \sum\limits_{k=0}^{p-1}\|H_k\rho-\pi_k\|_2^2 \le C_\varepsilon\ \}$, where C_ε depends on ε. Moreover, with additional assumptions on ε (see [16]) any sequence of solutions to $\min\limits_{\rho\in BV(\Omega)} F_\varepsilon(\rho)$ converges to a solution to $\min\{\|L\rho\|_2 \mid \rho\in BV(\Omega)\ , \sum\limits_{k=0}^{p-1}\|H_k\rho-\pi_k\|_2^2 = 0\}$, as $\varepsilon\to 0$.

Theorem 3.2 : *The minimization problem $(\mathcal{P})$ admits a unique solution.*

Proof : The proof is standard. Let (ρ_n) be a minimizing sequence of $BV(\Omega)$. Then $L\rho_n$ and ρ_n are bounded in $L^2(\Omega)$. As H_i is linear continuous from $L^2(\Omega)$ to $L^2(]-a,a[)$ it is weakly continuous as well and $H_i\rho_n-\pi_i$ weakly converges to $H_i\rho-\pi_i$ in $L^2(]-a,a[)$. The lower semi-continuity of the L^2 norm and the continuity of L give

$$F_\varepsilon(\rho) \le \liminf_{n\to\infty} F_\varepsilon(\rho_n).$$

Moreover, the sequence $(\Phi(\rho_n))$ is bounded as well. Since Ω is bounded, it follows that the sequence (ρ_n) is bounded in $BV(\Omega)$, and hence, up to a subsequence, it converges to some $\rho\in BV(\Omega)$ for the weak-star topology. The compact embedding property recalled in Proposition 3.1 implies that the sequence (ρ_n) converges strongly to ρ in $L^1(\Omega)$. Since Φ is lsc with respect to the $L^1(\Omega)$ topology, it follows that

$$\Phi(\rho) \le \liminf_{n\to\infty} \Phi(\rho_n).$$

Finally

$$J_\varepsilon(\rho) \le \liminf_{n\to\infty} J_\varepsilon(\rho_n) = \inf J_\varepsilon\ ,$$

and therefore ρ is a solution of $(\mathcal{P})$. Uniqueness is a consequence of the strict convexity of J_ε. □

We look now for optimality conditions and we need differentiability of the functional J_ε. It is clear that F_ε is differentiable and

$$\forall\rho\in L^2(\Omega)\quad \nabla F_\varepsilon(\rho) = \varepsilon L^*L\rho + \sum_{k=0}^{p-1} H_k^*\left(H_k\rho-\pi_k\right)\in L^2(\Omega)\ ,$$

where H_k^* is the adjoint operator of H_k. Unfortunately, the total variation $\Phi : BV(\Omega)\to\mathbb{R}$ is not differentiable. Therefore, we are going to investigate the dual problem (in the sense of convex analysis). We follow the method of Weiss et al. [28] to use a Nesterov-like algorithm to get the solution.

3.3. *Dual problem*

We first recall basic definitions and properties for convex duality.

Definition 3.3: Let $(E, \|.\|_E)$ be a Banach space and $T : E \longrightarrow \mathbb{R} \cup \{+\infty\}$ a convex function. The (Legendre-Fenchel) conjugate function of T is defined as

$$\begin{aligned} T^* : E' &\longrightarrow \mathbb{R} \cup \{+\infty\} \\ X &\longmapsto \sup_{x \in E} \{\langle X\ , x\rangle_E - T(x)\} \end{aligned}$$

where E' is the dual space of E and $\langle \cdot\ , \cdot \rangle_E$ denotes the duality bracket between E and E'.

We know ([14]) that if $T : E \longrightarrow \mathbb{R} \cup \{+\infty\}$ is a convex function then T^* is lower semi-continuous, and positively homogeneous. In addition, if T is lower semi-continuous then $T^{**} = T$.
Before we define the dual problem of $(\mathcal{P})$ we have to compute the conjugate functions of F_ε and Φ respectively.

Proposition 3.4: *The conjugate function of F_ε satisfies*

$$\forall \mu \in L^2(\Omega) \quad F_\varepsilon^*(\mu) = \left(\mu\ , A_\varepsilon^{-1}(\mu + \mathfrak{d})\right)_2 - F_\varepsilon\left(A_\varepsilon^{-1}(\mu + \mathfrak{d})\right). \tag{3.5}$$

where

$$A_\varepsilon = \left(\sum_{k=0}^{p-1} H_k^* H_k\right) + \varepsilon L^* L,\ \mathfrak{d} = \sum_{k=0}^{p-1} H_k^* \pi_k, . \tag{3.6}$$

Proof: For every $\mu \in L^2(\Omega)$, we have

$$F_\varepsilon^*(\mu) = \sup_{\rho \in L^2(\Omega)} \{(\mu, \rho)_2 - F_\varepsilon(\rho)\}.$$

The function $G_\varepsilon(\rho) := \rho \longmapsto (\mu, \rho)_2 - F_\varepsilon(\rho)$ is concave, differentiable and

$$\nabla G_\varepsilon(\rho) = \mu - \nabla F_\varepsilon(\rho).$$

The supremum of G_ε is obtained by solving $\nabla G_\varepsilon(\rho) = 0$, that is $\mu - \nabla F_\varepsilon(\rho) = 0$. So

$$\mu = \sum_{k=0}^{p-1} H_k^*(H_k \rho - \pi_k) + \varepsilon L^* L \rho.$$

Setting A_ε and $\mathfrak{d}$ as in (3.6) we have to solve

$$A_\varepsilon(\rho) = \mu + \mathfrak{d}\ . \tag{3.7}$$

System (3.7) has a unique solution for every $\mu \in L^2$ since the application $A_\varepsilon : L^2(\Omega) \to L^2(\Omega)$ is an isomorphism. Indeed, the continuity of the linear operator A_ε comes from the continuity of H_i, H_i^*, L and L^* and we get

$$\forall \rho \in L^2(\Omega) \qquad \varepsilon\kappa\|\rho\|_2^2 \leq (A_\varepsilon \rho\ , \rho)_2 \leq \|A_\varepsilon\|\|\rho\|_2^2\ . \tag{3.8}$$

This implies that A_ε is coercive and injective. Moreover, A_ε is self-adjoint so that $\varepsilon\kappa \leq \|A_\varepsilon^*\|$ as well. This gives the surjectivity of A_ε ([9] Theorem II.19) and we get $\|A_\varepsilon^{-1}\| \leq \frac{\kappa}{\varepsilon}$. The solution to (3.7) is $\rho_{\varepsilon,\mu} = A_\varepsilon^{-1}(\mu + \mathfrak{d})$ so that $F_\varepsilon^*(\mu)$ is given by relation (3.5). □

Proposition 3.5 [4, 10]**:** *The conjugate function of* Φ *is* $\Phi^* = \chi_{\overline{K}}$ *where* χ_C *is the characteristic function of a the subset* C *:* $\chi_C(\mu) = \begin{cases} 0 \text{ if } \mu \in C \\ +\infty \text{ else} \end{cases}$ *and* $\overline{K}$ *is the closure in* $L^2(\Omega)$ *of*

$$K = \left\{ h \mid \exists \psi \in C_c^1(\mathbb{R}^2, \mathbb{R}^2),\ \|\psi\|_\infty \leq 1,\ h = div\,\psi \right\}. \tag{3.9}$$

Now, we are ready to define the dual problem to $(\mathcal{P})$. First, we recall a generic convex duality result :

Theorem 3.6 : *[14] Let* X *be a normed space and* $f, g : X \longrightarrow \mathbb{R} \cup \{+\infty\}$ *convex functions such that there exists* $u_0 \in dom(g)$ *and* f *is continuous at* u_0*. Then*

$$\inf_{u \in X} (f(u) + g(u)) = \max_{v \in X'} (-f^*(v) - g^*(-v))$$

The dual problem $(\mathcal{P}^*)$ is then

$$(\mathcal{P}^*) \qquad \max_{\mu \in L^2(\Omega)} -F_\varepsilon^*(\mu) - \tau\Phi^*\left(-\frac{\mu}{\tau}\right) .$$

With proposition 3.5 $(\mathcal{P}^*)$ writes

$$(\mathcal{P}^*) : \max_{\mu \in \overline{K}} -F_\varepsilon^*(\mu) ,$$

where K is given by (3.9) and F_ε^* by (3.5).

Proposition 3.7: *The function* F_ε^* *is differentiable and*

$$\nabla F_\varepsilon^*(\mu) = A_\varepsilon^{-1}(\mu + \mathfrak{d}) . \tag{3.10}$$

Moreover, F_ε^* *is Lipschitz continuous with* $\dfrac{\kappa}{\varepsilon}$ *as a Lipschitz constant.*

Proof: The computation of ∇F_ε^* is easy with (3.5). In addition relation (3.8) yields that $\|A_\varepsilon^{-1}\| \leq \frac{\kappa}{\varepsilon}$. This ends the proof. □

3.4. *Nesterov algorithm*

We are now ready to use an algorithm by Y. Nesterov [23] to solve

$$\inf_{u \in Q} (\mathcal{E}(u)) \tag{3.11}$$

where $\mathcal{E} : \mathbb{R}^s \to \mathbb{R} \cup \{+\infty\}$ is a differentiable convex, α-Lipschitz function and Q is a closed convex subset of $\mathbb{R}^s$.

Definition 3.8: A function $d : \mathbb{R}^s \to \mathbb{R} \cup \{+\infty\}$ is a proximal function on Q if

- d is strongly convex: Q is differentiable and there exists $\sigma_Q > 0$ such that

$$\forall (u,v) \in Q \times Q \qquad (\nabla d(u) - \nabla d(v), u - v)_2 \geq \sigma_Q \|u - v\|_2^2 \ , \tag{3.12}$$

- there exists $u_0 \in Q$ such that

$$\forall v \in Q \qquad d(u) \geq \frac{\sigma_Q}{2} \|u - u_0\|_2^2 \ .$$

Let d_Q be a proximal function on Q. The algorithm is the following

Algorithm 3.1 Generic algorithm for problem (3.11)

Input : Maximum iterations number $nmax$ - starting point v_0
Output : u_{nmax} estimate of u^*
for $0 \leq k \leq nmax$ **do**
Compute $u_k = \underset{u \in Q}{\operatorname{argmin}} \left\{ (\nabla \mathcal{E}(v_k) \ , u - v_k)_2 + \frac{\alpha}{2} \|u - v_k\|_2^2 \right\}$
Compute $w_k = \underset{w \in Q}{\operatorname{argmin}} \left\{ \frac{\alpha}{\sigma_Q} d_Q(w) + \sum_{i=0}^{k} \frac{i+1}{2} \Big(\mathcal{E}(v_i) + (\nabla \mathcal{E}(v_i) \ , w - v_i)_2 \Big) \right\}$
Set $v_{k+1} = \frac{2}{k+3} w_k + \frac{k+1}{k+3} u_k$
end for

Theorem 3.9 : *([23], Th 2) Let $\{u_k\}_{k>0}$ be the sequence generated by the above algorithm and let u^* be the solution to problem* (3.11)*. Then for every $k > 0$*

$$0 \leq \mathcal{E}(u_k) - \mathcal{E}(u^*) \leq \frac{4\alpha d_Q(u^*)}{\sigma_Q (k+1)(k+2)}.$$

Following [28] we use this scheme to solve the dual problem $(\mathcal{P}^*)$. Here $\mathcal{E} = F_\varepsilon^*$ and $Q = \overline{K}$. A classical choice for d_K is $d_K(u) = \frac{1}{2}\|u\|_2^2$ with $u_0 = 0$ and $\sigma_K = 1$.

4. Numerical realization

In what follows we consider that three data sets are available ($p = 3$) corresponding to angles $\theta_0 = 0$, $\theta_1 = \frac{\pi}{2}$ and $\theta_2 = \frac{\pi}{4}$. With the previous notations

$$H_0 := H_{\theta=0}, \quad H_1 := H_{\theta=\frac{\pi}{2}} \text{ and } H_2 := H_{\theta=\frac{\pi}{4}} \ .$$

Moreover, for sake of simplicity we choose $L = Id_{L^2(\Omega)}$. However, any convolution operator can be handled very easily using the Fast Fourier Transform.

4.1. *Discretization process*

The discretization process is standard. Fix $N \in \mathbb{N}$ and choose a uniform grid on $[-a, a] \times [-a, a]$ whose nodes are $(x_k, y_l)_{1 \leq k,l \leq N}$. The discretization step is $h := 2a/N$ so that

$$x_k = -a + kh = \frac{2k - N}{N} a, \quad y_\ell = -a + \ell h = \frac{2\ell - N}{N} a \qquad k, \ell = 0, \cdots, N \ .$$

We approximate functions by piecewise constant functions that are identified to $\mathbb{R}^{N^2}$ vectors. In the sequel, we denote similarly $L^2(\Omega)$ functions (resp. $L^2(]-a,a[)$ functions) and their discrete approximation in $\mathbb{R}^{N^2}$ (resp. in $\mathbb{R}^N$). We set $X := \mathbb{R}^{N^2}$ and $Y := X \times X$. For $s \in \{N, N^2\}$, the space $\mathbb{R}^s$ is endowed with the classical inner product and the induced euclidean norm. More precisely, we use the usual norms in Y

$$\|u\|_1 = \sum_{i,j=1}^{N} \left(|u^1_{i,j}| + |u^2_{i,j}|\right) \ , \|u\|_2 = \left(\sum_{i,j=1}^{N} |u_{i,j}|_2^2\right)^{\frac{1}{2}} \quad , \quad \|u\|_\infty = \max_{1\le i,j\le N} |u_{i,j}|_2$$

where $u = (u^1, u^2) \in Y$ and $|u_{i,j}|_2 := \sqrt{(u^1_{i,j})^2 + (u^2_{i,j})^2}$, $1 \le i, j \le N$.
The gradient of ρ is approximated as $(\nabla_h \rho)_{i,j} = \left((\nabla_h\rho)^1_{i,j}, (\nabla_h\rho)^2_{i,j}\right)$ with a forward scheme

$$(\nabla_h\rho)^1_{i,j} = \begin{cases} \dfrac{\rho_{i+1,j} - \rho_{i,j}}{h} & \text{if } i < N \\ 0 & \text{if } i = N \end{cases} \text{ and } (\nabla_h\rho)^2_{i,j} = \begin{cases} \dfrac{\rho_{i,j+1} - \rho_{i,j}}{h} & \text{if } j < N \\ 0 & \text{if } j = N \end{cases} \tag{4.13}$$

and the discrete divergence operator writes

$$\forall \mu = (\mu^1, \mu^2) \in Y \qquad (\mathrm{div}_h \mu)_{i,j} = \frac{\left((d_1\mu^1)_{i,j} + (d_2\mu^2)_{i,j}\right)}{h}$$

where a backward scheme is used :

$$(d_1\mu^1)_{i,j} = \begin{cases} \mu^1_{i,j} - \mu^1_{i-1,j} & \text{if } 1 < i < N \\ \mu^1_{i,j} & \text{if } i = 1 \\ -\mu^1_{i,j} & \text{if } i = N \end{cases} \text{ and } (d_2\mu^2)_{i,j} = \begin{cases} \mu^2_{i,j} - \mu^2_{i,j-1} & \text{if } 1 < j < N \\ \mu^2_{i,j} & \text{if } j = 1 \\ -\mu^2_{i,j} & \text{if } j = N \end{cases} \tag{4.14}$$

4.1.1. Discrete form of the projection operators.

Recall that

$$H_\theta\rho(y) = \int_{-\infty}^{+\infty} 1_\Omega(x,y)\rho(x\cos\theta + y\sin\theta, -x\sin\theta + y\cos\theta)\, dx.$$

• We first compute H_0 for $\theta = 0$. For every $y \in]-a, a[$ we get

$$H_0\rho(y) = \int_{-\infty}^{+\infty} 1_\Omega(x,y)\rho(x,y)dx = \int_{-a}^{a} 1_{[-\sqrt{a^2-y^2}, \sqrt{a^2-y^2}]}(x)\rho(x,y)\, dx.$$

Let us set

$$M_{k,\ell} = \begin{cases} h & \text{if } x_k^2 + y_\ell^2 \le a^2 \\ 0 & \text{else} \end{cases} = h \begin{cases} 1 & \text{if } (2k-N)^2 + (2\ell - N)^2 \le N^2 \\ 0 & \text{else} \end{cases}$$

Therefore

$$\forall \ell \in \{1, \cdots, N\} \qquad H_0\rho(y_\ell) \simeq H_0\rho(\ell) := \sum_{k=1}^{N} M_{k,\ell}\, \rho(k,\ell)\ . \tag{4.15}$$

• Case $\theta = \dfrac{\pi}{2}$. We use the same reasoning to get

$$\forall k \in \{1, \cdots, N\} \qquad H_1\rho(x_k) \simeq H_1\rho(k) := \sum_{\ell=1}^{N} M_{\ell,k}\, \rho(k,\ell)\ . \tag{4.16}$$

• Case $\theta = \dfrac{\pi}{4}$. The detector has to be discretized in a different way because it is not parallel to the axis of the cartesian grid. Let $z_1, \cdots, z_{2N-1}$, be an uniform grid on the detector with step $\tilde{h} = \dfrac{h}{\sqrt{2}}$ and $z_N = 0$ so that

$$\forall \ell \in \{1, \cdots, 2N-1\} \qquad z_\ell = (\ell - N)\tilde{h} = \frac{(\ell - N)h}{\sqrt{2}} = \frac{(\ell - N)}{N}\sqrt{2}a\ .$$

For every ℓ such that $|z_\ell| \leq a$, we get

$$H_2\rho(z_\ell) = \int_{-\sqrt{a^2 - z_\ell^2}}^{\sqrt{a^2 - z_\ell^2}} \rho\left(\frac{x + z_\ell}{\sqrt{2}}, \frac{-x + z_\ell}{\sqrt{2}}\right) dx = \sqrt{2} \int_{\frac{-\sqrt{a^2 - z_\ell^2} + z_\ell}{\sqrt{2}}}^{\frac{\sqrt{a^2 - z_\ell^2} + z_\ell}{\sqrt{2}}} \rho\left(x, -x + \sqrt{2}z_\ell\right) dx\ .$$

A simple computation gives

$$\forall \ell \in \{1, \cdots, 2N-1\} \quad |z_\ell| \leq a \iff N\left(1 - \frac{\sqrt{2}}{2}\right) \leq \ell \leq N\left(1 + \frac{\sqrt{2}}{2}\right)\ .$$

In the sequel we denote

$$\mathcal{I}_N = \left\{ \ell \in \mathbb{N} \mid N(1 - \frac{\sqrt{2}}{2}) \leq \ell \leq N(1 + \frac{\sqrt{2}}{2}) \right\} (\subset \{1, \cdots, 2N-1\})\ .$$

Setting $x = -a + th$ we get

$$H_2\rho(z_\ell) = h\sqrt{2} \int_{\frac{\ell - \sqrt{\frac{N^2}{2} - (\ell - N)^2}}{2}}^{\frac{\ell + \sqrt{\frac{N^2}{2} - (\ell - N)^2}}{2}} \rho\left(-a + th, -a + (\ell - t)h\right)\, dt\ .$$

Finally, for every $\ell \in \mathcal{I}_N$

$$\begin{aligned} H_2\rho(z_\ell) &= h\sqrt{2} \int_0^N 1_{[\frac{\ell - \sqrt{\frac{N^2}{2} - (\ell - N)^2}}{2}, \frac{\ell + \sqrt{\frac{N^2}{2} - (\ell - N)^2}}{2}]}(t) \rho\left(-a + th, -a + (\ell - t)h\right)\, dt \\ &= h\sqrt{2} \sum_{k=1}^{N} \int_{k-1}^{k} 1_{[\frac{\ell - \sqrt{\frac{N^2}{2} - (\ell - N)^2}}{2}, \frac{\ell + \sqrt{\frac{N^2}{2} - (\ell - N)^2}}{2}]}(t) \rho\left(-a + th, -a + (\ell - t)h\right)\, dt\ . \\ &\simeq h\sqrt{2} \sum_{k=1}^{N} 1_{[\frac{\ell - \sqrt{\frac{N^2}{2} - (\ell - N)^2}}{2}, \frac{\ell + \sqrt{\frac{N^2}{2} - (\ell - N)^2}}{2}]}(k) \rho(k, \ell - k). \end{aligned}$$

For every $\ell \in \{1, \cdots, 2N-1\}$ and $k \in \{1, \cdots, N\}$, set

$$\begin{aligned}\widetilde{M}_{k,\ell} &= \begin{cases} h\sqrt{2} & \text{if } |\ell - 2k| \leq \sqrt{\frac{N^2}{2} - (\ell - N)^2} \text{ and } \ell \in \mathcal{I}_N \\ 0 & \text{else} \end{cases} \\ &= h\sqrt{2} \begin{cases} 1 & \text{if } (2k-\ell)^2 + (\ell - N)^2 \leq \frac{N^2}{2} \\ 0 & \text{else} \end{cases}\end{aligned}$$

$$\forall \ell \in \{1, \cdots, 2N-1\} \qquad H_2\rho(z_\ell) \simeq H_2\rho(\ell) := \sum_{k=1}^{N} \widetilde{M}_{k,l}\, \rho(k, \ell - k)\ . \tag{4.17}$$

4.1.2. Discrete form of the adjoint operators.

We compute first H_0^* and H_1^*: let be $u \in X$ and $w \in \mathbb{R}^N$:

$$\begin{aligned}(H_0 u, w)_{\mathbb{R}^N} &= \sum_{\ell=1}^{N} (H_0 u)(\ell) w(\ell) = \sum_{\ell=1}^{N} \sum_{k=1}^{N} M_{k,\ell}\, u(k,\ell) w(\ell) \\ &= \sum_{\ell,k=1}^{N} u(k,\ell) M_{k,\ell}\, w(\ell)\ .\end{aligned}$$

So

$$\forall k, \ell \in \{1, \cdots, N\} \qquad (H_0^* w)(k,\ell) = M_{k,\ell}\, w(\ell)\ .$$

Similarly

$$\forall k, \ell \in \{1, \cdots, N\} \qquad (H_1^* w)(k,\ell) = M_{\ell,k}\, w(k)\ .$$

Let us compute H_2^* : let be $u \in X$ and $w \in \mathbb{R}^{2N-1}$:

$$\begin{aligned}(H_2 u, w)_{\mathbb{R}^{2N-1}} &= \sum_{\ell=1}^{2N-1} (H_2 u)(\ell) w(\ell) = \sum_{\ell=1}^{2N-1} \sum_{k=1}^{N} \widetilde{M}_{k,\ell}\, u(k, \ell - k) w(\ell) \\ &= \sum_{k=1}^{N} \sum_{p=1-k}^{2N-1-k} u(k,p) \widetilde{M}_{k,p+k}\, w(p+k)\ .\end{aligned}$$

So

$$\forall k, p \in \{1, \cdots, N\} \qquad (H_2^* w)(k,p) = \widetilde{M}_{k,p+k}\, w(p+k)\ .$$

4.2. *Nesterov algorithm*

The discrete problem reads

$$(\mathcal{P}_h) \ : \ \inf_{\rho \in X} F_h(\rho) + \tau \|\nabla_h \rho\|_1 \tag{4.18}$$

where F_h is a discrete approximation of F and ∇_h is a discrete gradient (see (4.13)). More precisely we may define F_h as

$$F_h(\rho) = \frac{1}{2}\sum_{k=0}^{2} \|H_k\rho - \pi_k\|_2^2 + \frac{\varepsilon}{2}\|\rho\|_2^2$$

where $\|.\|_2$ is either the ℓ^2- norm in $\mathbb{R}^N$ (for H_0 and H_1) , the ℓ^2 -norm in $\mathbb{R}^{2N-1}$ (for H_2) or the ℓ^2- norm in $\mathbb{R}^{N^2}$. The dual problem writes

$$(\mathcal{P}_h^*) \ : \ \inf_{q\in Y} F_h^*(-\mathrm{div}_h(q)) + \tau\ell_1^*(-\frac{q}{\tau}) \tag{4.19}$$

where F_h^* is the F_h conjugate function, ℓ_1^* is the conjugate function of the ℓ_1 -norm ($\|\cdot\|_1$) and div_h is the discrete divergence operator in (4.14).
The following result has been proved in [28]

Theorem 4.1 : *The dual problem is equivalent to*

$$\inf_{q\in K_\tau} (F_h^*(-div_h(q))) \tag{4.20}$$

with $K_\tau = \{q \in Y, \|q\|_\infty \leq \tau\}$. *The application* $q \mapsto F_h^*(-div(q))$ *is* α *-Lipschitz continuous and differentiable, with* $\alpha = \frac{2\|div_h\|_2^2}{\sigma}$ *(here* σ *is the* F_h *strong convexity coefficient as in Definition* (3.12)*).*
The solution $\bar{\rho}$ *to the primal problem satisfies*

$$\bar{\rho} = \nabla F_h^*(-div_h(\bar{q})),$$

where $\bar{q}$ *is the solution to the dual problem.*

In the sequel Π_{K_τ} is the orthogonal projection on the set K_τ. The solution to problem (4.20) is computed with Algorithm (3.11), $\mathcal{E} = F_h^* \circ (-\mathrm{div})$, $Q = K_\tau$, $d_Q = \frac{1}{2}\|\cdot - \xi_0\|_2^2$, where $\xi_0 \in Q$. This gives

Algorithm 4.1 Algorithm to solve problem (4.20)

Input : Iterations number J - starting point $\xi_0 \in K_\tau$
Output : q_J approximation of $\bar{q}$

Set $\alpha = 2\|\mathrm{div}_h\|_2^2$
Set $G_{-1} = 0$
for $0 \leq k \leq J$ **do**
$\eta_k = \nabla_h\big(\nabla F_h^*(-\mathrm{div}_h(\xi_k))\big)$
$q_k = \Pi_{K_\tau}\left(\xi_k - \dfrac{\eta_k}{\alpha}\right)$
$G_k = G_{k-1} + \dfrac{k+1}{2}\eta_k,\ \nu_k = \Pi_{K_\tau}\left(\xi_0 - \dfrac{G_k}{\alpha}\right).$
$\xi_{k+1} = \dfrac{2}{k+3}\nu_k + \dfrac{k+1}{k+3}q_k$
end for

4.3. *Implementation*

We apply Algorithm (4.1) to our problem to obtain

Algorithm 4.2 Algorithm for problem (4.19)

Input : Iterations number : J - Number of views : p
Angles : $(\theta_0, ..., \theta_{p-1})$ - Data : $(\pi_0, \dots, \pi_{p-1})$
- starting point $\xi_0 \in K_\tau$
Set $\alpha = 8/\varepsilon$.
Output : q_J approximation of $\bar{q}$

Compute $A_\varepsilon := \displaystyle\sum_{k=0}^{p-1} H_k^* H_k + \varepsilon I_{N^2}$ and $\mathfrak{d} = \displaystyle\sum_{k=0}^{p-1} H_k^* \pi_k$;
Set $G_{-1} = 0$
for $1 \leq \ell \leq J$ **do**

1. Compute μ_ℓ the solution to

$$A_\varepsilon \, \mu_\ell = -\mathrm{div}_h(\xi_\ell) + \mathfrak{d} \tag{4.21}$$

2. $\eta_\ell = \nabla_h \mu_\ell$
3. $q_\ell = \Pi_\tau \left(\xi_\ell - \dfrac{\eta_\ell}{\alpha} \right)$
4. $G_\ell = G_{\ell-1} + \dfrac{\ell+1}{2} \eta_\ell$.
5. $\nu_\ell = \Pi_\tau \left(\xi_0 - \dfrac{G_\ell}{\alpha} \right)$.
6. $\xi_{\ell+1} = \dfrac{2}{\ell+3} \nu_\ell + \dfrac{\ell+1}{\ell+3} q_\ell$

end for

Here I_{N^2} stands for the $N^2 \times N^2$ identity matrix and Π_τ is the ℓ^∞ projection on a ℓ^2 ball of radius τ : $\Pi_\tau(V)_i = \begin{cases} V_i & \text{if } |V_i|_2 \leq \tau \\ \tau \frac{V_i}{|V_i|_2} & \text{else} \end{cases}$.
The (approximate) solution $\rho_J \simeq \bar{\rho}$ of problem (4.18) is

$$\rho_J = \nabla F_h^*(-\mathrm{div}_h(q_J) + \mathfrak{d})$$

where q_J is an approximate solution $\bar{q}$ of problem (4.19) computed by Algorithm (4.2). Practically we solve once again system (4.21)

$$A_\varepsilon \, \rho_J = -\mathrm{div}_h(q_J) + \mathfrak{d} \ .$$

5. Numerical results

5.1. *Test image and data*

We consider an academic test object whose size is 256× 256 pixels. The different components are geometric objets with arbitrary uniform density. The (simulated) projection data are presented in next figure :

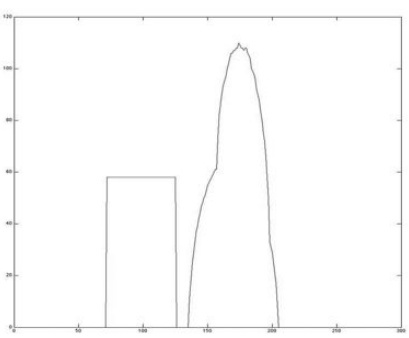

(a) $\theta = \frac{\pi}{2}$

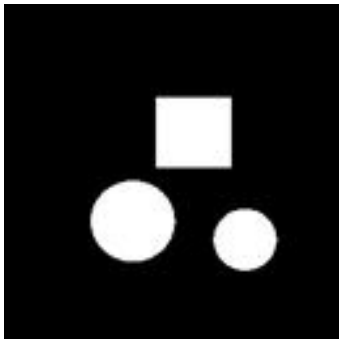

(b) Original test image

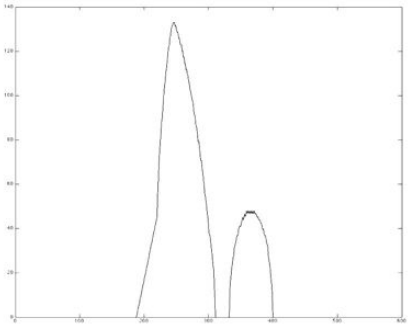

(c) $\theta = \frac{\pi}{4}$

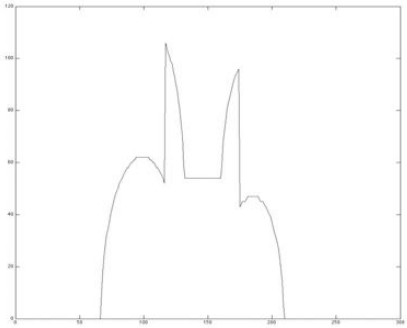

(d) $\theta = 0$

Figure 5.1. Test image and projection data

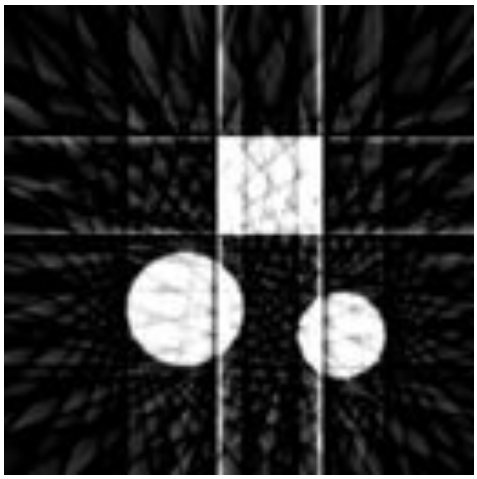

(a) Reconstruction with 18 views

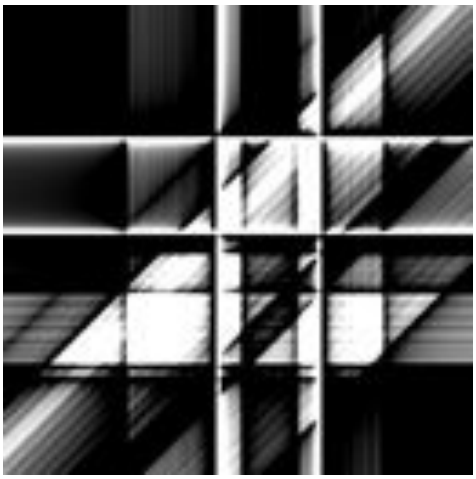

(b) Reconstruction with angles 0, $\pi/4$ and $\pi/2$

Figure 5.2. Reconstruction with filtered-back projection formula for data without noise (Ram-Lak filter with a Hann window and spline interpolation)

As expected the classical filtered-back projection gives very bad results because of the very few number of available data. Figure 5.2 presents the reconstruction with a Rak-Lam filter and a Hann window.

The tests have been performed using MATLAB©. The prescribed tolerance ε_{tol} is equal to 10^{-4} and $N_{max} = 2000$. The accuracy for the conjugate gradient loop has been set to 10^{-3} and the number of iterations limited to $N(= 256)$.

5.2. *Noiseless reconstruction*

5.2.1. Sensitivity with respect to ε

We first consider the case of noiseless data (which is unrealistic of course). Theoretically, the parameter ε should be chosen as small as possible, but the problem turns to be unstable (A_ε is ill-conditioned) if ε is too small. The numerical results for different values $\varepsilon = 10^{-s}, s = 0, \cdots, 4$ (see figure below) lead to the choice $\varepsilon = 0.1$ or $\varepsilon = 0.01$.

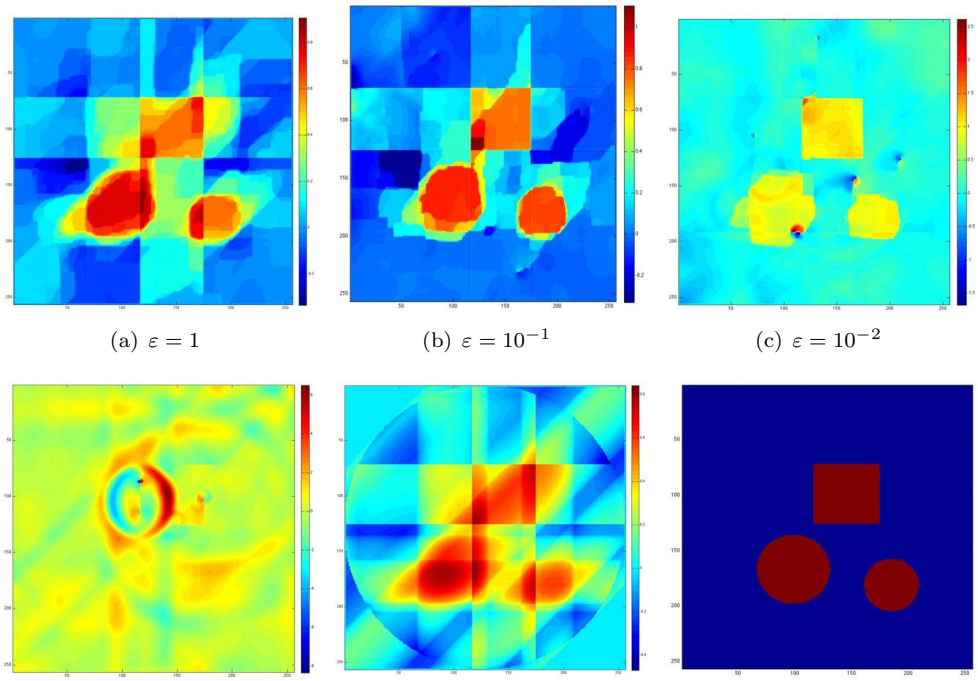

(a) $\varepsilon = 1$ (b) $\varepsilon = 10^{-1}$ (c) $\varepsilon = 10^{-2}$

(d) $\varepsilon = 10^{-3}$ (e) $\varepsilon = 10^{-4}$ (f) Original

Figure 5.3. Noiseless data - sensitivity with respect to ε - $\tau = 15$

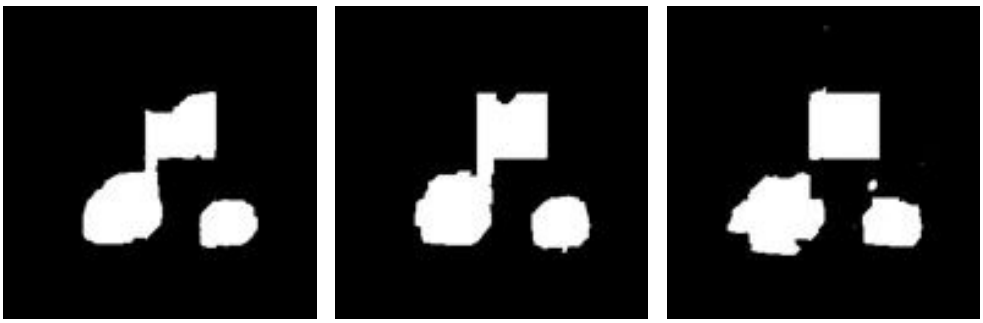

(a) $\varepsilon = 1$ (b) $\varepsilon = 10^{-1}$ (c) $\varepsilon = 10^{-2}$

Figure 5.4. Noiseless data - sensitivity with respect to ε - $\tau = 15$ - binary threshold : 0.5

We call ρ_{orig} the original image and ρ_τ the computed solution. We report in Table 5.2.1,

- $F_\varepsilon(\rho_{orig})$ and $F_\varepsilon(\rho_\tau)$,
- $\Phi(\rho_{orig})$ and $\Phi(\rho_\tau)$, the respective total variation
- the L^2- norm of the solution,

- the relative fitting data term

$$\mathbf{e}_\tau = \frac{\sum \|H_k\ \rho_\tau - \pi_k\|_2^2}{\sum \|\pi_k\|_2^2}$$

- the relative error :

$$\mathfrak{e} := \frac{\|\rho_{orig} - \rho_\tau\|_2}{\|\rho_{orig}\|_2}$$

- the number of iterations, and
- the CPU-time. As we have not optimized the codes, the absolute CPU time makes no sense. We report here the CPU time to give a relative information.

	$\varepsilon = 1$	$\varepsilon = 10^{-1}$	$\varepsilon = 10^{-2}$	$\varepsilon = 10^{-3}$	$\varepsilon = 10^{-4}$
$F_\varepsilon(\rho_{orig})$	2.31 e+03	2.31 e+02	2.31 e+01	2.31	2.31 e-01
$F_\varepsilon(\rho_\tau)$,	2.21 e+03	3.76 e+02	2.08 e+02	3.68 e+02	26.01
$\Phi(\rho_\tau)$	1.49 e-02	1.64 e-02	3.06 e-02	11.9 e-02	1.99 e-01
$\mathbf{e}_\tau$	1.5 e-04	8.3 e-05	8.9 e-05	1.7 e-04	1.2 e-05
$\|\rho_\tau\|_2$	9.4 e-04	9.7 e-04	1 e-03	2.2 e-03	9.4 e-04
$\mathfrak{e}$	5.54 e-01	3.64 e- 01	2.98 e-01	19.1 e-01	6.1 e-01
Iterations number	961	1707	1776	1538	1972
CPU time $/10^4$ (s)	2.76	6.73	8.44	7.31	9

Table 5.2.1. Sensitivity with respect to ε - Noiseless data - $\tau = 15$ - $\Phi(\rho_{orig}) = 1.02e-02, \sum \|\pi_k\|_2^2 = 2.07e+06$.

The above results clearly show the instability effects when ε is too small.

5.2.2. Sensitivity with respect to τ

We report the different errors in next table :

τ	$F_\varepsilon(\rho_\tau)$	$\Phi(\rho_\tau)$	$\|\rho_\tau\|_2$	$\mathbf{e}_\tau$	$\mathfrak{e}$	It.	CPU time (s)
5	2.73 e+02	1.58 e-02	9.5 e-04	3.7 e-05	0.497	1570	6.21 e+04
15	3.76 e+02	1.64 e-02	9.75 e-04	8.27 e-05	0.365	1707	6.73 e+04
25	6.04 e+02	1.56 e-02	9.94 e-04	1.88 e-04	0.261	1587	6.65 e+04
35	7.56 e+02	2.09 e-02	9.82 e-04	2.64 e-04	0.317	1546	6.72 e+04
40	8.17 e+02	1.78e-02	9.87 e-04	2.92 e-04	0.284	2000	8.68 e+04
50	10.4 e+02	1.84 e-02	9.99 e-04	3.99 e-04	0.292	1583	6.8 e+04
60	11 e+02	1.80 e-02	9.9 e-04	3.8 e-04	0.275	1782	7.68 e+04
70	13.7 e+02	2.16 e-02	9.88 e-04	5.6 e-04	0.337	1676	7.19 e+04

Table 5.2.2. Sensitivity with respect to τ - Noiseless data - $\varepsilon = 0.1$ - $F_\varepsilon(\rho_{orig}) = 2.31e+02$ and $\Phi(\rho_{orig}) = 1.02e-02$.

Figure 5.5 shows the solutions for $\varepsilon = 0.1$ and different values of the regularization parameter τ.

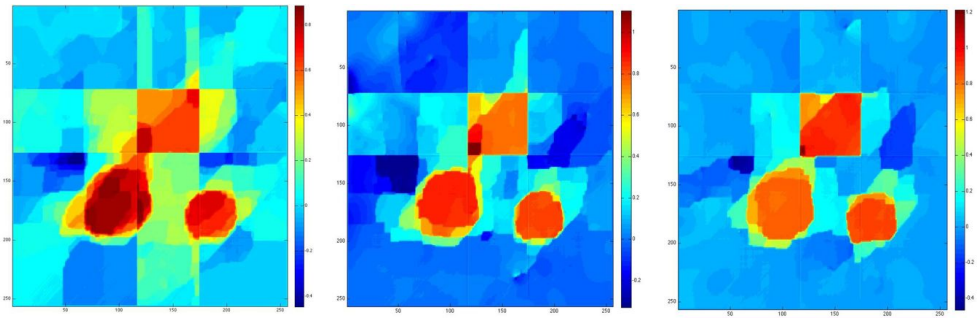

(a) $\tau = 5$ (b) $\tau = 15$ (c) $\tau = 25$

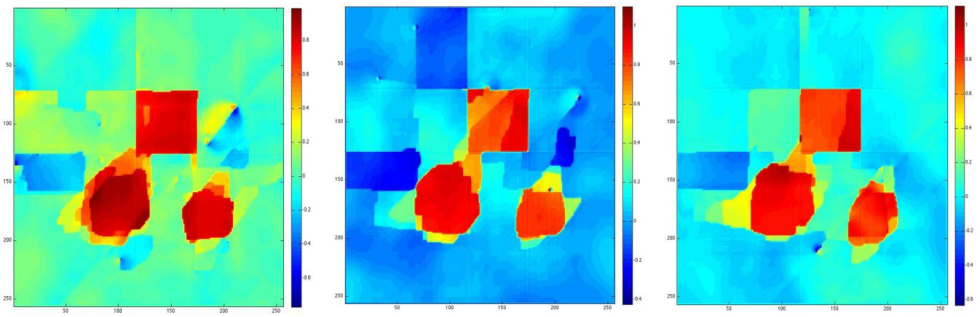

(d) $\tau = 35$ (e) $\tau = 50$ (f) $\tau = 60$

Figure 5.5. Noiseless data - $\varepsilon = 0.1$ - sensitivity with respect to τ

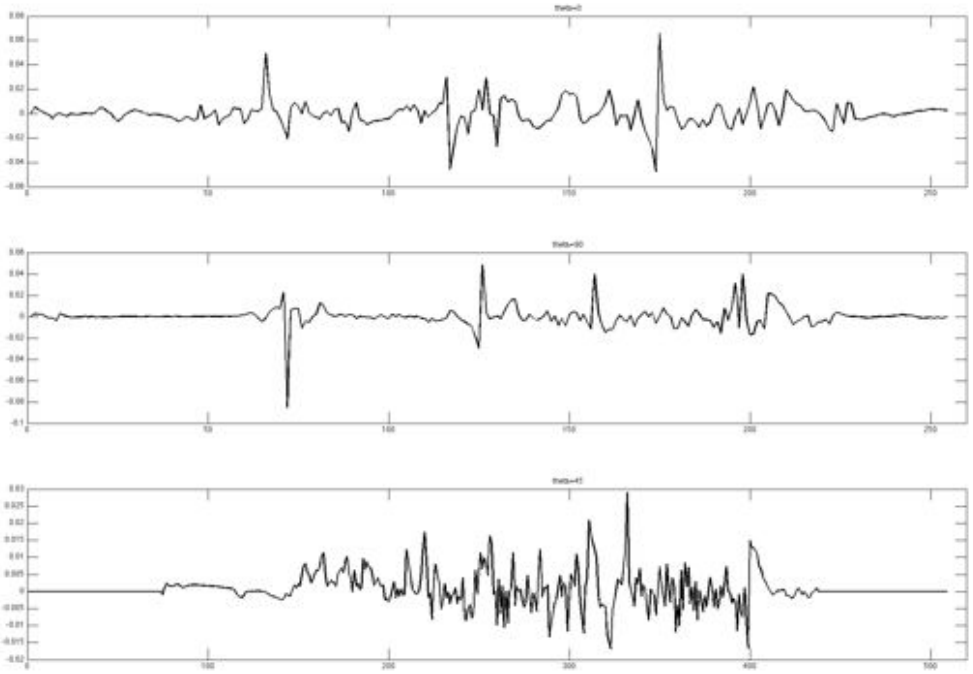

Figure 5.6. Noiseless data - $\varepsilon = 0.1$, $\tau = 25$ - Normalized errors $(H_k(\rho_\tau) - \pi_k)/\max|\pi_k|$ between the projections of the solution and the (exact) data.

We note that the original object does not minimize the cost functional F_ε, at last for small τ. This comes from the modelling feature : the model we chose is not realistic enough. We have to look for another model that takes into account more accurately the physical context. Moreover, the best results are obtained with

small values of τ. This was predictable: in case the data are noiseless, the total variation penalization term is not useful (since there is no noise to remove). The total variation weight should quite small since the most important part of the functional F is the fitting data term.

We note that the reconstruction is not satisfying : we get an ellipse (with a small excentricity parameter along the axis $\theta = \frac{\pi}{4}$) instead of a disk. Indeed such an object has projections very close to the ones of the original disk. It is hopeless to get a nice reconstruction without additional prior that allows to control this kind of perturbations. Other affects (blur) are related to the large value of τ. In that case, the optimal solution is far from the original solution.

5.3. *Case where data are noisy*

Now we consider noisy data: we have added to the "exact" (simulated) projection a gaussian white noise with standard deviation σ. We present results for $\sigma = 0.05$ (Figure 5.6).

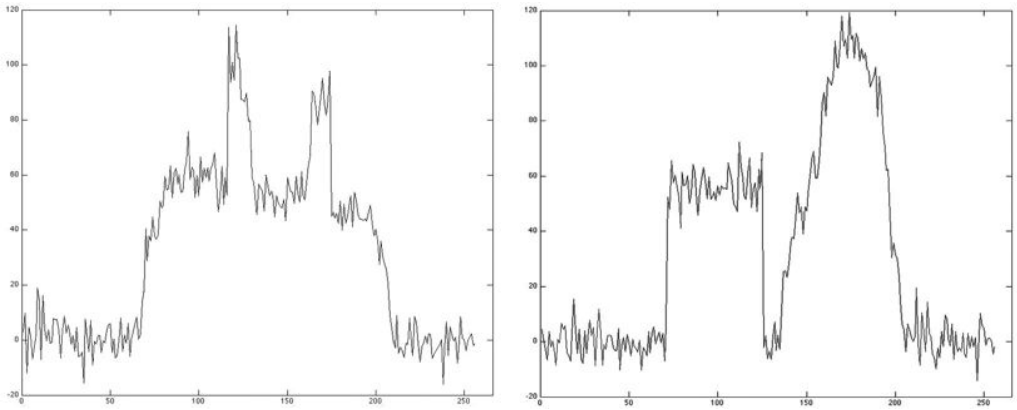

(a) $\theta = 0$ (b) $\theta = \frac{\pi}{2}$

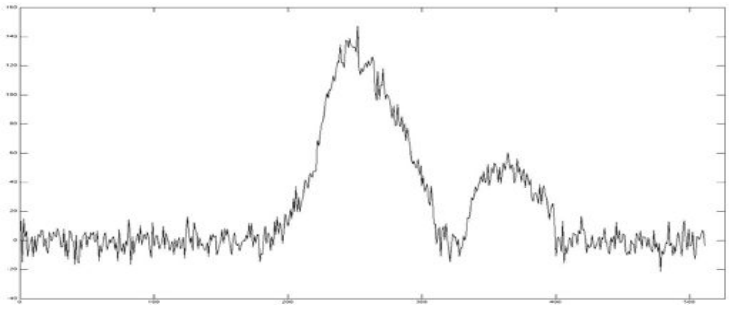

(c) $\theta = \frac{\pi}{4}$

Figure 5.7. Noisy data - Gaussian noise with $\sigma = 0.05$

We report in next table the quantitative behaviour of the solutions. We have added the Signal to Noise Ratio, that we define here as

$$SNR_\tau = \log_{10}\left(\frac{\sum_i \|H_i\rho_\tau\|_2^2}{\sum_i \|H_i(\rho_\tau - \rho_{orig})\|_2^2}\right).$$

Indeed, the noise can only be observed on the data and the relevance of the solution

is measured via its projections. Next figure shows different solutions for $\varepsilon = 1$ and different τ values:

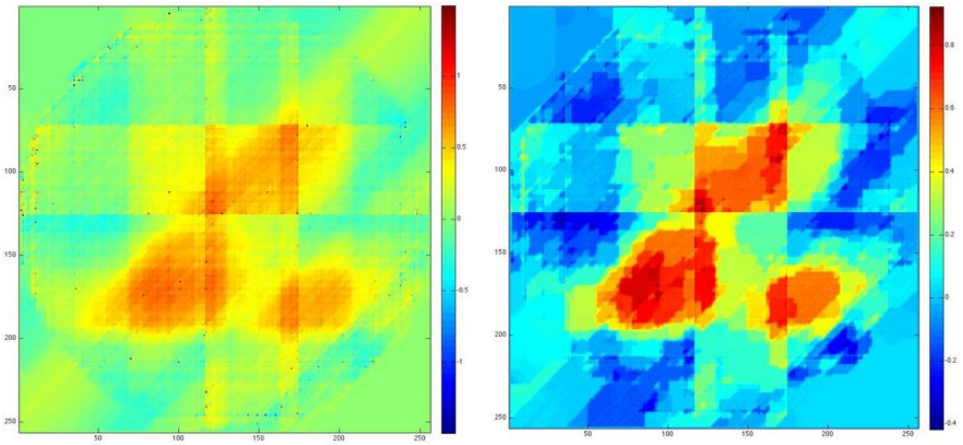

(a) $\tau = 1$

(b) $\tau = 15$

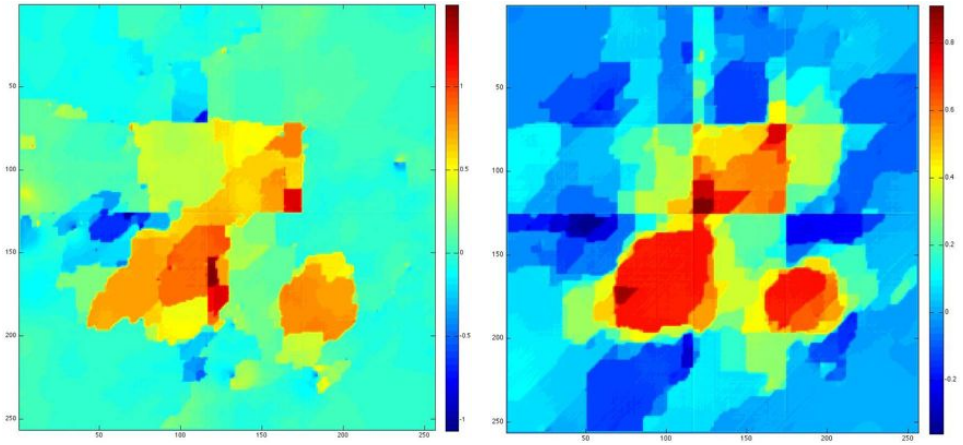

(c) $\tau = 35$

(d) $\tau = 45$

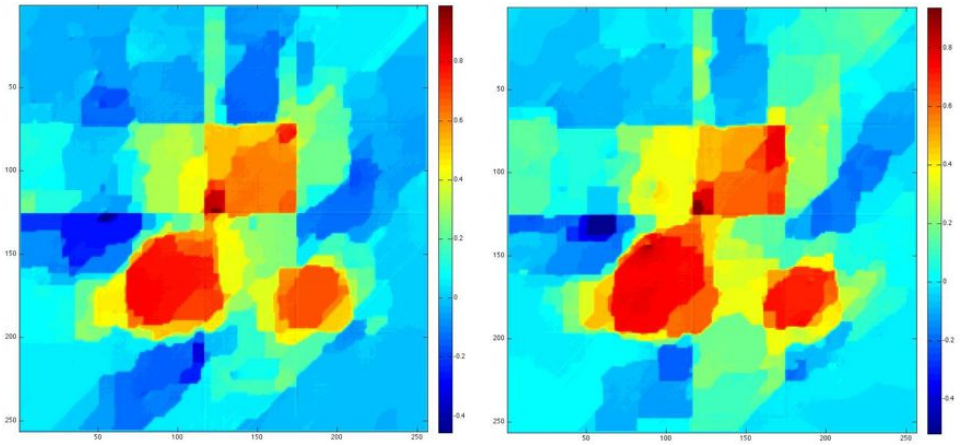

(e) $\tau = 55$

(f) $\tau = 65$

Figure 5.8. Reconstruction with noisy data - $\varepsilon = 1$ – $\sigma = 0.05$

	$\tau = 1$	$\tau = 15$	$\tau = 25$	$\tau = 35$	$\tau = 45$	$\tau = 55$	$\tau = 65$
$F_\varepsilon(\rho_\tau)$	5.57 e+03	1.05 e+04	1.29 e+04	1.45 e+04	1.54 e+04	1.63 e+04	1.69 e+04
$\Phi(\rho_\tau)$	6.12 e-02	3.21 e-02	2.49 e-02	2.14 e-02	1.95 e-02	1.86 e-02	1.82 e-02
$\mathbf{e}_\tau$	3.6 e-03	8.3 e-03	1.05 e-02	1.2 e-02	1.29 e-02	1.37 e-02	1.43 e-02
$\mathfrak{e}$	0.6	0.57	0.56	0.53	0.55	0.51	0.53
SNR	2.43	2.07	1.97	1.91	1.87	1.85	1.83
# iterations	224	660	803	942	1158	1198	1228
CPU time (s)	9.11 e+03	2.4 e+04	2.8 e+04	3.26 e+04	3.9 e+04	4.12 e+04	4.3 e+04

Table 5.3.1. Noisy data reconstruction ($\sigma = 0.05$) - $\varepsilon = 1$ - Sensitivity to τ - $F_\varepsilon(\rho_{orig}) = 2.07\,e+04,\ \Phi(\rho_{orig}) = 1.02\,1e-02$

Next figures show the projections of the computed object with respect to the observed (noisy) projections and to the exact one.

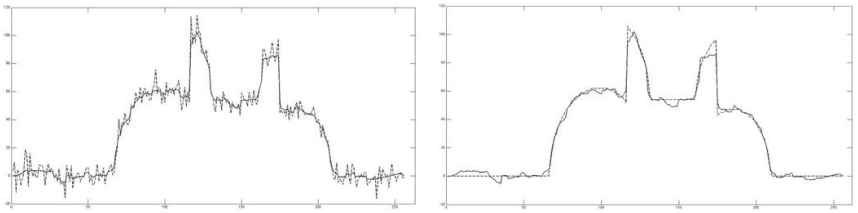

(a) Computed solution (continuous line) and noisy data (dotted line) - $\theta = 0$

(b) Computed solution (continuous line) and exact data (dotted line) - $\theta = 0$

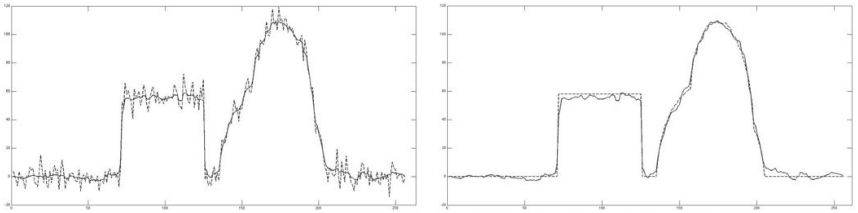

(c) Computed solution (continuous line) and noisy data (dotted line)- $\theta = \pi$

(d) Computed solution (continuous line) and exact data (dotted line) - $\theta = \pi$

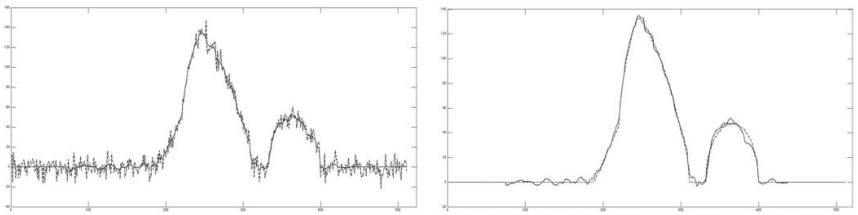

(e) Computed solution (continuous line) and noisy data (dotted line) - $\theta = \pi/2$

(f) Computed solution (continuous line) and exact data (dotted line) - $\theta = \pi/2$

Figure 5.9. Comparison between computed, observed and exact projections - $\sigma = 0.05,\ \varepsilon = 1,\ \tau = 55$

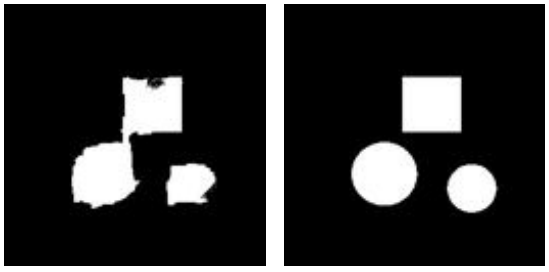

(a) Solution - Threshold 0.5

(b) Original

Figure 5.10. Reconstruction with noisy data - $\varepsilon = 1\ -\ \sigma = 0.05\ -\ \tau = 55$ - Thresholded solution (threshold =0.5)

The sensitivity to parameter τ is an important point. If τ is too small, we cannot get rid of the noise efficiently. If it is too large the computed solution is far from the (real) expected one. The parameter τ has to be related to the noise level. Next figure presents the evolution of SNR_τ with respect to τ for different values of σ

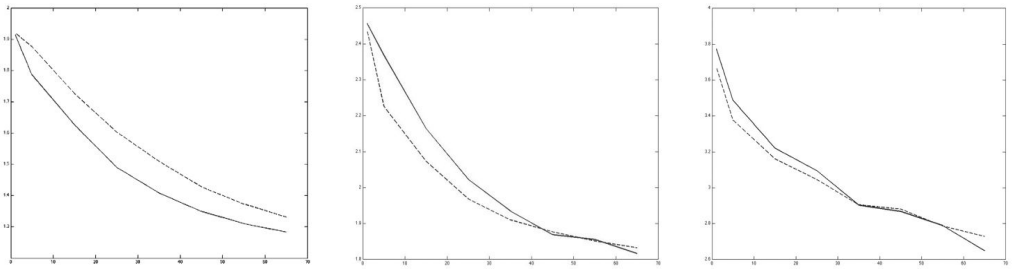

(a) SNR - $\sigma = 0.1$ (b) SNR - $\sigma = 0.05$ (c) SNR - $\sigma = 0.01$

Figure 5.11. SNR behavior with respect to τ and different σ, $\varepsilon = 1$ (dotted line) and $\varepsilon = 0.1$ (continuous line)

6. Conclusion

The variational model allows to get acceptable results for a severely ill posed problem . However, the penalization term $\frac{\varepsilon}{2}\|L\rho\|_2^2$ is not physically realistic if we choose $L = Id$. The choice of L as high-pass or low-pass filter allows to add priors on the reconstructed object : we may decide to recover specific frequencies of the object . The numerical scheme has to be improved as well : the resolution of the linear system (4.21), $A_\varepsilon \mu = \mathfrak{b}$ should be faster. It may be performed using a Choleski decomposition of A_ε if we get performant hardware. It should be interesting as well to use a new efficient primal-dual algorithm [11] that is a good alternative to the Nesterov method.

At last, we need to add priors on the object to let the model more precise and realistic. In practise, the object is "almost" axisymmetric and could be recovered using a deformation from a symmetric one. One can recover a symmetric object from the available data with techniques of [1, 8] . Then we may look for a deformation vector field that drives the axisymmetric object to the non symmetric one. This point of view will be studied in a forthcoming work.

References

[1] R. Abraham, M. Bergounioux, and E. Trélat, *A penalization approach for tomographic reconstruction of binary axially symmetric objects*, Applied Mathematics and Optimization (2008), no. 58:345-371.
[2] R. Acar and C.R. Vogel, *Analysis of bounded variation penalty methods for ill-posed problems*, Inverse Problems 10 (1994), no. 6:1217–1229.
[3] L. Ambrosio, N. Fusco, and D. Pallara, *Functions of bounded variation and free discontinuity problems*, Clarendon Press – Oxford, 2000.
[4] J.F. Aujol, *Some first-order algorithms for total variation based image restoration*, J Math Imaging Vis (2009), no. 34: 307-327.
[5] K.J. Batenburg, *Reconstructing binary images from discrete x-rays*, Tech. report, Leiden University, The Netherlands, 2004.
[6] ———, *A network flow algorithm for binary image reconstruction from few projections*, (2006), no. 4245:6–97.
[7] R.H.T. Bates, K.L. Garden, and T.M. Peters, *Overview of computerized tomography with emphasis on future developments*, Proeedings IEEE, vol. 71, 1983, pp. 256–297.
[8] M. Bergounioux and E. Trélat, *A variational method using fractional order hilbert spaces for tomographic reconstruction of blurred and noised binary images*, Journal of Functional Analysis (2010), no. 259: 2296–2332.
[9] H. Brézis, *Analyse fonctionnelle, théorie et aplications*, Dunod-Masson, 1987.
[10] A. Chambolle, *An algorithm for total variation minimization and applications*, Journal of Mathematical Imaging and Vision (2004), no. 20:89–97.

[11] A. Chambolle and T. Pock, *A first-order primal-dual algorithm for convex problems with applications to imaging*, J. Math. Imaging Vision (2011), no. 40 (1):120–145.
[12] M. Courdurier, F. Noo, M. Defrise, and H. Kudo, *Solving the interior problem of computed tomography using a priori knowledge*, Inverse Problems (2008), no. 24.
[13] N.J. Dusaussoy, *Image reconstruction from projections*, SPIE's international symposium on optics, imaging and instrumentation, San Diego, 1984.
[14] I. Ekeland and R. Temam, *Convex analysis and variational problems*, SIAM Classic in Applied Mathematics, 28, 1999.
[15] G. Herman, *Image reconstruction from projections: the fundamentals of computerized tomography*, Academic Press, 1980.
[16] B. Hofmann, B. Kaltenbacher, C. Pöschl, and O. Scherzer, *A convergence rates result for tikhonov regularization in banach spaces with non-smooth operators*, Inverse Problems (2007), no. 23:987–1010.
[17] Y. L. Hstao, G.T. Herman, and T. Gabor, *A coordinate ascent approach to tomographic reconstruction of label images from a few projections*, (2005), no. 151:184-197.
[18] ———, *Discrete tomography withj a very few views, using gibbs priors and a marginal posterior mode approach*, (2005), no. 20:399-418.
[19] J.-M.Dinten, *Tomographie à partir d'un nombre limité de projections : régularisation par des champs markoviens*, Ph.D. thesis, Université de Paris–Sud, 1990.
[20] A. Kirsch, *An introduction to the mathematical theory of inverse problems*, Springer-verlag, New York, 1996.
[21] F. Natterer, *The mathematics of computerized tomography*, SIAM, 2001.
[22] F. Natterer and F. Wübeling, *Mathematical methods in image reconstruction*, SIAM, 2001.
[23] Y. Nesterov, *Smooth minimization of non-smooth functions*, Mathematic Programming, Ser. A (2005), no. 103:127-152.
[24] F. Noo, R. Clackdoyle, and J.D. Pack, *A two-step hilbert transform method for 2d image reconstruction*, Physics in Medicine and Biology (2004), no. 49(17):3903-3923.
[25] D. Partouche-Sebban and I. Abraham, *Scintillateur pour dispositif d'imagerie, module scintillateur, dispositif d'imagerie avec un tel scintillateur et procédé de fabrication d'un scintillateur*, French patent no 2922319, April 2009.
[26] D. Partouche-Sebban, I. Abraham, S. Lauriot, and C.Missault, *Multi-mev flash radiography in shock physics experiments: Specific assemblages of monolithic scintillating crystals for use in ccd-based imagers*, X-Ray Optics and Instrumentation (2010), Article ID 156984– 9p.
[27] E.T. Quinto, *Singularities of the x-ray transform and limited data tomography in* $\mathbb{R}^2$ *and* $\mathbb{R}^3$, SIAM J. Math. Anal. (1993), no. 24:1215-1225.
[28] P. Weiss, G. Aubert, and L.Blanc-Féraud, *Efficient schemes for total variation minimization under constraints in image processing*, SIAM Journal on Scientific Computing (2009), no. 31 (3):2047–2080.